BIOCELL

Tech Science Press

Doi:10.32604/biocell.2025.060411

ARTICLE

# Mistletoe Lectin Induces Apoptosis and Modulates the Cell Cycle in YD38 Oral Squamous Cell Carcinoma Cells

**Chang-Eui Hong**[1] **and Su-Yun Lyu**[2,*]

[1]Department of Pharmacy, Sunchon National University, Sunchoeon, 57922, Republic of Korea
[2]Institute of Life and Pharmaceutical Sciences, Sunchon National University, Suncheon, 57922, Republic of Korea

*Corresponding Author: Su-Yun Lyu. Email: suyun@scnu.ac.kr

Received: 31 October 2024; Accepted: 03 January 2025; Published: 28 February 2025

**ABSTRACT: Objectives:** Despite progress in therapeutic interventions, squamous cell carcinoma of the oral cavity (OSCC) continues to pose a substantial burden on public health, with persistently poor patient outcomes. This investigation examines the growth-inhibitory and mechanistic effects of a plant-derived protein, *Viscum album* var. *coloratum* agglutinin (VCA), extracted from Korean mistletoe, against YD38 OSCC cells. **Methods:** The experimental protocols involved treating YD38 cells derived from human OSCC with escalating doses of VCA. Cell survival rates were quantified through 3-(4,5-dimethylthiazol-2-yl)-2,5-diphenyltetrazolium bromide (MTT) colorimetric analysis. Changes in apoptotic indices and cell cycle distribution were evaluated using flow cytometric techniques. Protein expression patterns associated with programmed cell death were determined via Western blot analysis. Statistical evaluation including effect size calculations, dose-response modeling, and correlation analyses were conducted to comprehensively evaluate VCA's effects. **Results:** VCA exhibited dose-dependent cytotoxicity against YD38 cells. Flow cytometry analysis revealed significant increases in both early and late apoptotic populations at 100 and 1000 ng/mL VCA, with Cohen's $d$ values of 15.15 and 30.24, respectively, indicating large biological effects. Cell cycle analysis showed significant alterations in cell cycle distribution, and Western blot analysis demonstrated increased levels of cleaved poly (ADP-ribose) polymerase (PARP) and cleaved caspase-3, indicating activation of the caspase-dependent apoptotic pathway. Correlation analysis revealed strong relationships between different cellular responses ($r > 0.95$), suggesting coordinated cellular responses to VCA treatment. **Conclusion:** This study demonstrates that VCA exhibits potent anti-cancer effects against YD38 OSCC cells through apoptosis induction and cell cycle modulation, with quantitative analyses revealing strong effect sizes and coordinated cellular responses. These results add to our understanding of natural compounds in oncology and indicate that VCA could be a promising candidate in OSCC treatment development.

**KEYWORDS:** Mistletoe; YD38; apoptosis; cell cycle

## 1 Introduction

Oral squamous cell carcinoma (OSCC) represents a significant healthcare challenge worldwide, ranking as the sixth leading malignancy globally. An estimate 389,846 new cases of OSCC are attributed to OSCC in 2022 [1]. This comprises a varied set of tumors affecting various regions in the mouth's cavity, which include the lips, tongue, gums, floor of mouth, and the salivary glands [2]. Multiple risk determinants contribute to OSCC development, encompassing both inherited susceptibilities and lifestyle exposures. Smoking habits, chronic alcohol intake, and human papillomavirus (HPV) infections—particularly in oropharyngeal malignancies—serve as primary risk factors [3–6]. Despite advances in cancer therapeutics, the management

of OSCC remains challenging. The current standard of care generally consists of a multimodal approach, which combines surgery, radiation therapy, and chemotherapy. However, these treatments often result in significant morbidity, including facial disfigurement, speech impairment, and difficulty in swallowing, severely impacting patients' quality of life [7–9]. Moreover, the five-year survival rate for squamous cell carcinoma has remained stubbornly low, hovering around 50% for the past several decades, with limited improvement despite therapeutic advancements [1,10]. This persistent challenge underscores the urgent need for novel therapeutic strategies that may enhance therapeutic efficacy and patients' well-being.

The exploration of natural compounds has gained considerable traction in cancer research, offering a vast and diverse chemical space with unique structural features that often differ from synthetic molecules [11]. These substances have been a rich source of medicinal agents throughout human history and remain essential in therapeutic development. In the field of oncology research, natural compounds offer several advantages, including the potential to act on multiple cellular targets simultaneously, a characteristic that aligns well with the complex and multifaceted nature of cancer [12,13]. Among these natural sources, mistletoe extracts have emerged as a subject of intense scientific scrutiny, particularly in the field of complementary and alternative medicine for cancer treatment. Mistletoe (*Viscum album* L.) has a long history of use in traditional medicine and has gained significant attention in contemporary cancer research [14]. The therapeutic potential of mistletoe is attributed to its diverse bioactive compounds, including lectins (ML-I, ML-II, and ML-III), viscotoxins, alkaloids, flavonoids, and phenylpropanoids [15].

Of particular interest is the Korean mistletoe (*V. album* var. *coloratum*), which has shown promising results in several cancer models, making it an intriguing candidate for investigation in OSCC treatment. This subspecies of European mistletoe contains unique lectins, particularly *V. album* var. *coloratum* agglutinin (VCA), a type 2 ribosome-inactivating protein (RIP) consisting of an enzymatic N-glycosidase A subunit and a sugar-binding B subunit connected via disulfide bonding that may contribute to its anti-cancer properties [16]. VCA has been found to have distinct characteristics compared to lectins from European mistletoe, including differences in sugar-binding specificity and biological activities. Specifically, VCA shows preferential binding to N-acetylgalactosamine-containing glycoconjugates and exhibits more potent cytotoxicity compared to European mistletoe lectins [17]. Studies on VCA have demonstrated its potential anti-cancer effects in various cancer types. The mechanisms by which VCA exerts its anti-cancer properties are still being explored, however, multiple pathways have been identified. VCA has been demonstrated to cause apoptosis through both intrinsic and extrinsic mechanisms, modify cell cycle progression, and influence various signaling processes involved in the survival and growth of cells [18]. Additionally, like other mistletoe lectins, VCA has demonstrated immunomodulatory properties, which could contribute to its overall anti-cancer effects [19–21]. Despite these promising findings, the effects of VCA on squamous cell carcinoma, particularly the YD38 human OSCC cell line, have not been thoroughly investigated. Given the pressing need for new therapeutic strategies in OSCC treatment, exploring the potential of VCA in this context could provide valuable insights and potentially lead to novel treatment approaches.

For investigating OSCC molecular mechanisms, validated cancer cell models provide valuable tools for studying the molecular mechanisms underlying cancer progression and response to potential therapies. YD38 cell line is a useful model for oral cancer research that was derived from a moderately differentiated squamous cell carcinoma of the lower gingiva of a 67-year-old Korean male patient [22]. This cell line is part of the Cancer Dependency Map project (DepMap), including the Cancer Cell Line Encyclopedia (CCLE) [23,24], indicating its significance in large-scale cancer research efforts. YD38 cells harbor a homozygous nonsense mutation in the TP53 gene (p.Gly199Ter), resulting in a non-functional p53 protein [25], a characteristic often associated with more aggressive cancer phenotypes. With extensive omics data available, including deep exome and transcriptome analyses [26], YD38 provides a valuable tool for studying the effects

of potential therapeutic agents on OSCC and integrating findings with broader cancer research initiatives. However, it's important to acknowledge that single-cell line models may not fully represent the heterogeneity observed in clinical tumors. Therefore, findings from YD38 cells should be interpreted cautiously and ideally validated across multiple cell lines or in more complex model systems [27].

While earlier investigations have documented the antineoplastic activities of multiple botanical lectins, most have focused primarily on qualitative or semi-quantitative analyses. The need for a more rigorous quantitative assessment of lectin effects has been increasingly recognized in cancer research [28]. Comprehensive statistical analyses, including effect size calculations, dose-response modeling, and correlation studies, can provide deeper insights into the biological significance and mechanistic relationships of observed effects [29]. Such quantitative approaches are particularly valuable in evaluating potential therapeutic agents, as they can help establish dose-response relationships, determine effect magnitudes, and reveal coordinated cellular responses that might not be apparent from conventional analyses alone [30].

The present study aims to investigate the effects of Korean mistletoe lectin on YD38 cells. By examining changes in cell viability, apoptosis induction, cell cycle progression, and molecular pathway activation, combined with comprehensive statistical analyses including effect size calculations, dose-response modeling, and correlation studies, we seek to gain insights into the potential anti-cancer properties of this natural compound. This multi-parameter quantitative approach allows for a more rigorous evaluation of VCA's therapeutic potential, providing not only mechanistic insights but also robust statistical evidence for its effects. These observations could advance the establishment of novel therapeutic strategies for OSCC, addressing the pressing need for more effective and less toxic treatment options. Furthermore, our quantitative framework may serve as a valuable model for future investigations into utilizing naturally occurring lectins as precision therapeutics and adjuvants in oral cancer treatment.

## 2 Materials and Methods

### *2.1 Preparation of VCA from Korean Mistletoe*

Plant material was harvested from mistletoe growing as a parasitic plant on Quercus species in the mountainous regions of Kangwon province, Republic of Korea. The plant tissues consisting of mature leaves, berries, and stems (1–4 years old) were harvested in winter and authenticated by Prof. Jong Suk Lee at the College of Natural Sciences, Seoul Women's University, Republic of Korea. All plant materials were maintained at −70°C for preservation until further processing. For initial extraction, the plant material was mechanically processed using a specialized dual-roller vegetable processor (Angel Life Co., Pocheon, Republic of Korea) with phosphate-buffered saline (PBS, pH 7.4, Sigma, P4474, St. Louis, MO, USA) at a ratio of 1:10 (w/v). This homogenate was passed through decreasing pore size filters (60, 25, 10, 5, 2, and 0.22 μm, Cytiva, Marlborough, MA, USA), and was then centrifuged at 12,000 rpm (VS-550, Vision Scientific Co., Daejeon, Republic of Korea) for 30 min at 4°C to remove cellular debris. Using previously described cation exchange chromatography [31], the crude protein solution was isolated. Protein samples were analyzed using sodium dodecyl sulfate-polyacrylamide gel electrophoresis (SDS-PAGE) in both reducing and non-reducing environments showing the purity and identification of VCA. VCA was seen as a single band at 60 kDa in non-reducing settings and as A and B chains at 34 and 31 kDa, respectively, with purity >95% as measured by densitometric analysis (Fig. A1) under reducing conditions. Protein content was quantitated using the bicinchoninic acid (BCA) assay (Sigma, BCA1). The enzyme-linked lectin assay (ELLA) method was utilized to determine the lectin content.

### *2.2 Cell Culture and Viability Assay*

YD38 OSCC cells (RRID: CVCL_L083) were supplied from the Korean Cell Line Bank (Seoul, Republic of Korea). The cells were maintained in Roswell Park Memorial Institute (RPMI) 1640 (Sigma, R8758) supplemented with 10% (v/v) fetal bovine serum (FBS, 16000044, Life Technologies, Carlsbad, CA, USA), 1% (v/v) non-essential amino acids (Sigma, M7145), 1% (v/v) L-glutamine (Sigma, G7513), and 1% (v/v) penicillin-streptomycin (Sigma, P0781) at 37°C, 5% $CO_2$ in a humidified atmosphere. Human oral keratinocytes (HOK) were purchased from the American Type Culture Collection (ATCC, PCS-200-014, Carlsbad, CA, USA). Dermal cell basal medium (ATCC, PCS-200-030) combined with keratinocyte growth kit components (ATCC, PCS-200-040) was used to maintain cells at 37°C under a humidified atmosphere and 5% $CO_2$. Mycoplasma contamination of the cell line was routinely tested using the MycoAlert™ Mycoplasma Detection Kit (Lonza, LT07-318, Basel, Switzerland), and no contamination was observed during the course of this study. The 3-(4,5-dimethylthiazol-2-yl)-2,5-diphenyltetrazolium bromide (MTT, Sigma, M5655) assay was used to determine cell viability. YD38 cells were seeded in 96 well plates at the density of $5 \times 10^3$ cells per well and exposed to different doses of VCA (0–1000 ng/mL) for 48 h in a complete medium consisting of 10% FBS, 1% non-essential amino acids, 1% L-glutamine, and 1% penicillin streptomycin. Physiologically relevant conditions and maintaining optimum cell viability during the treatment period was achieved by the use of complete medium. After treatment, 10 µL MTT solution (5 mg/mL in PBS) was put into each well and the plates were then incubated for a further 4 h. The medium was aspirated carefully and the particles of formazan were dispersed in 100 µL of dimethyl sulfoxide (DMSO, Sigma, D8418) per well. The microplate was measured at 570 nm (630 nm as the reference wavelength) with a microplate reader (Tecan, Sunrise™, Männedorf, Switzerland). Viability of the cells was expressed as a percentage of the untreated control group.

### *2.3 Apoptosis Analysis*

Apoptosis in YD38 cells was assessed using the Muse™ Annexin V and Dead Cell Assay Kit (EMD Millipore, MCH100105, Billerica, MA, USA). VCA treated cells were cultured for 48 h. Cells have been obtained and prepared in accordance with the manufacturer's instructions following treatment. In brief, 100 µL of treated cell suspension ($1 \times 10^5$ cells/mL) was added to 100 µL of Muse™ Annexin V and Dead Cell Reagent (EMD Millipore, part number 4700–1485). In the dark, the blend was allowed to stand at room temperature for 20 min. The samples were then analyzed on the Muse™ Cell Analyzer (EMD Millipore, 0500-3115) after incubation. Percentages of live, early apoptotic, late apoptotic/dead, and dead cells were quantified using the instrument. Data acquisition and analysis were done with the Muse™ Annexin V and Dead Cell software module (EMD Millipore). In each experiment, a triplicate was performed.

### *2.4 Cell Cycle Analysis*

The Muse™ Cell Cycle Assay Kit (EMD Millipore, MCH100106) was used to analyze cell cycle dispersion following the supplier's protocol. YD38 cells were incubated with VCA for 48 h. Cells were gathered after treatment, rinsed with PBS and kept in ice-cold 70% ethanol at –20°C overnight. The preserved cells were washed on the day of analysis with PBS to remove ethanol and incubated with Muse™ Cell Cycle Reagent (EMD Millipore, part number. 4700–1495) for 30 min at room temperature in darkness. The Muse™ Cell Analyzer (EMD Millipore, 0500-3115) was employed to analyze the labeled cells. Data acquisition and computer processing was performed using Muse™ Cell Cycle software module (EMD Millipore) to calculate the percent of cells in G0/G1, S, and G2/M stages of the cell cycle. All experiments were carried out in triplicate.

### *2.5 Western Blotting*

Western blot analysis was employed to investigate the production of apoptosis associated proteins. We incubated YD38 cells with VCA for 48 h. Protein was seperated in radio-immunoprecipitation assay (RIPA) lysis buffer (Thermo Fisher Scientific, 89900, Waltham, MA, USA) containing protease and phosphatase inhibitors (Thermo Fisher Scientific, 78444). Protein concentrations were quantified with the BCA Protein Assay kit (ThermoFisher scientific, 23227). SDS-PAGE was performed to separate proteins (30 μg per lane) and transferred to polyvinylidene fluoride (PVDF) membranes (Millipore EMD, IPVH00010). Membranes were blocked with 5% non-fat milk in tris-buffered saline with 0.1% Tween-20 Detergent (TBS-T, Sigma, P1379) at room temperature for 1 h. Afterwards, the membranes underwent incubation overnight at 4 degress Celsius with primary antibodies against cleaved poly (ADP-ribose) polymerase (PARP, 1:1000, Cell Signaling Technology, Danvers, MA, USA), caspase-3 (1:1000, Cell Signaling Technology, 9662), cleaved caspase-3 (1:1000, Cell Signaling Technology, 9661), and glyceraldehyde-3-phosphate dehydrogenase (GAPDH, 1:1000, Cell Signaling Technology, 5174). After washing with TBS-T, the membranes were incubated with horseradish peroxidase (HRP)-conjugated secondary antibodies (1:2000, Cell Signaling Technology, 7074) for 1 h at room temperature. The protein bands were detected using an enhanced chemiluminescence (ECL) detection system (GE Healthcare, RPN2109, Chicago, IL, USA). Quantification of band intensities was carried out in ImageJ software (NIH, version 1.54k, Bethesda, MD, USA) and normalized to GAPDH. All experiments were performed in triplicate.

### *2.6 Heatmap Analysis*

Gene expression data from Western blotting experiments were used to generate a heatmap. $Log_2$ fold changes relative to the control were calculated for each gene across all treatment conditions. The heatmap was created using Microsoft Excel (Microsoft Corporation, LTSC Professional Plus 2021, Redmond, WA, USA) with conditional formatting. Genes were clustered based on similarity in expression patterns across treatments. The color scale was set to diverge from white (no change) to red (upregulation), with the intensity of the color representing the magnitude of change.

### *2.7 Statistical Analyses and Data Visualization*

Data are displayed as mean ± SD of every study carried out in triplicate. GraphPad Prism software (version 8.0, GraphPad Software, San Diego, CA, USA) was applied for the statistical evaluations. Multiple groups have been assessed through one way analysis of variance (ANOVA) followed by Tukey's post hoc test. The analysis of the data was conducted using principal component analysis (PCA) applied with the R statistical software (version 4.1.0). Pearson correlation coefficient was employed to generate correlation matrices. Effect sizes were determined utilizing Cohen's $d$ to characterize the amount of changes between treatment groups, with values interpreted into three catagories: minor effect ($0.2 \leq d < 0.5$), medium effect ($0.5 \leq d < 0.8$), and large effect ($d \geq 0.8$). Dose-response curves were generated for cell viability, apoptosis induction, and G0/G1 phase distribution. The relationships between VCA concentration and various cellular responses were analyzed using non-linear regression analysis with a four-parameter logistic equation. The general form of the equation used was: $Y = Bottom + (Top-Bottom)/(1 + (X/K)^{HillSlope})$ in which Y is the reaction, X is the VCA dose, Bottom is the lowest reaction, Top is the highest reaction, K is a fitting constant, and HillSlope describes the steepness of the curve.

## 3 Results

### *3.1 Effect of VCA on YD38 Cell Viability*

Growth inhibitory properties of VCA were analyzed in YD38 cells via metabolic assessment. Exposure of cells to increasing concentrations of VCA (0–1000 ng/mL, 48 h) revealed dose-related changes in cellular health. Initial doses showed minimal impact, with 1 and 10 ng/mL treatments maintaining cellular integrity at 100.00 ± 2.14% and 89.73 ± 3.87%, respectively, showing no statistical difference from baseline controls ($p > 0.05$). The first notable decline emerged at 100 ng/mL, where cell health decreased to 81.06 ± 8.32% ($p < 0.01$). Progressive concentration increases led to further reductions, reaching 49.94 ± 10.25% ($p < 0.001$) at 1000 ng/mL and 44.18 ± 2.96% ($p < 0.001$) at maximal exposure (10,000 ng/mL). For subsequent investigations, 100 ng/mL was identified as optimal, representing the minimum concentration yielding significant biological effects while preserving sufficient cell population for detailed analyses. The 1000 ng/mL concentration was selected as it achieved approximately 50% reduction in cell viability, a commonly used threshold in cytotoxicity studies. These two concentrations allow us to examine the effects of VCA at both a moderate and a more potent dose while avoiding potential non-specific effects that might occur at higher concentrations, thereby providing insights into the dose-dependent nature of VCA's anti-cancer effects.

Fig. 1A illustrates the dose-dependent reduction in cell viability induced by VCA. To evaluate potential cytotoxicity against normal cells, we examined the effect of VCA on human oral keratinocytes (HOK) (Fig. 1B). Importantly, HOK cells maintained >99% viability at VCA concentrations up to 1000 ng/mL, while significant cytotoxicity was only observed at much higher concentrations (86.68 ± 6.52% viability at 10,000 ng/mL and 21.62 ± 2.31% at 100,000 ng/mL). These results suggest that VCA exhibits selective toxicity on cancer cells with little impact on normal oral epithelial cells at therapeutically relevant concentrations.

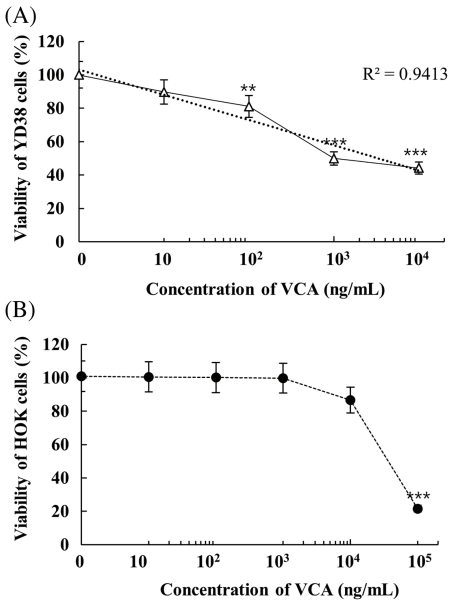


**Figure 1:** Growth response analysis of *Viscum album* var. *coloratum* agglutinin (VCA) treatment. (A) YD38 human oral squamous cell carcinoma (OSCC) cells and (B) non-malignant human oral keratinocytes (HOK) were exposed to varying concentrations of VCA for a 48-h period, after which cellular metabolic activity was evaluated using the 3-(4,5-dimethylthiazol-2-yl)-2,5-diphenyltetrazolium bromide (MTT) colorimetric method. Values represent mean ± standard deviation (SD) from three independent experiments. Asterisks denote significant differences from untreated controls: $^{**}p < 0.01$, $^{***}p < 0.001$ (one-way ANOVA followed by Tukey's post-hoc test)

### *3.2 Programmed Cell Death Analysis in VCA-Treated YD38 Cells*

Analysis using dual-staining with Annexin V and 7-aminoactinomycind D (7-AAD) demonstrated that VCA triggers programmed cell death pathways. The flow cytometry results showed progressive increases in phosphatidylserine externalization and membrane permeability at both 100 and 1000 ng/mL concentrations (Fig. 2A,B). These concentration-dependent changes in cellular markers indicate that regulated cell death is the predominant response to VCA exposure. Baseline measurements in vehicle-treated populations showed 6.2 ± 0.4% cells displaying early membrane changes (Annexin V-positive/7-AAD-negative) and 3.4 ± 0.3% cells with compromised membrane integrity (Annexin V/7-AAD double-positive). The total apoptotic population (early + late) in control cells was 9.6 ± 0.7%. Treatment with 100 ng/mL VCA significantly increased the early apoptotic population to 11.5 ± 0.6% ($p < 0.001$) and the late apoptotic/dead population to 12.8 ± 0.8% ($p < 0.001$). The total apoptotic population at this concentration was 24.3 ± 1.2% ($p < 0.001$). At 1000 ng/mL VCA, the early apoptotic population further increased to 20.1 ± 0.9% ($p < 0.001$), and the late apoptotic/dead population reached 26.7 ± 1.1% ($p < 0.001$). The total apoptotic population at this highest concentration was 46.8 ± 1.6% ($p < 0.001$). Concurrently, the percentage of live cells (Annexin V-/7-AAD-) decreased from 89.8 ± 1.2% in the control to 73.9 ± 1.5% at 100 ng/mL VCA ($p < 0.001$) and 51.6 ± 1.8% at 1000 ng/mL VCA ($p < 0.001$). The dead cell population (Annexin V-/7-AAD+) showed a slight but significant increase from 0.6 ± 0.1% in control to 1.8 ± 0.3% at 100 ng/mL VCA ($p < 0.01$) and 1.6 ± 0.2% at 1000 ng/mL VCA ($p < 0.01$).

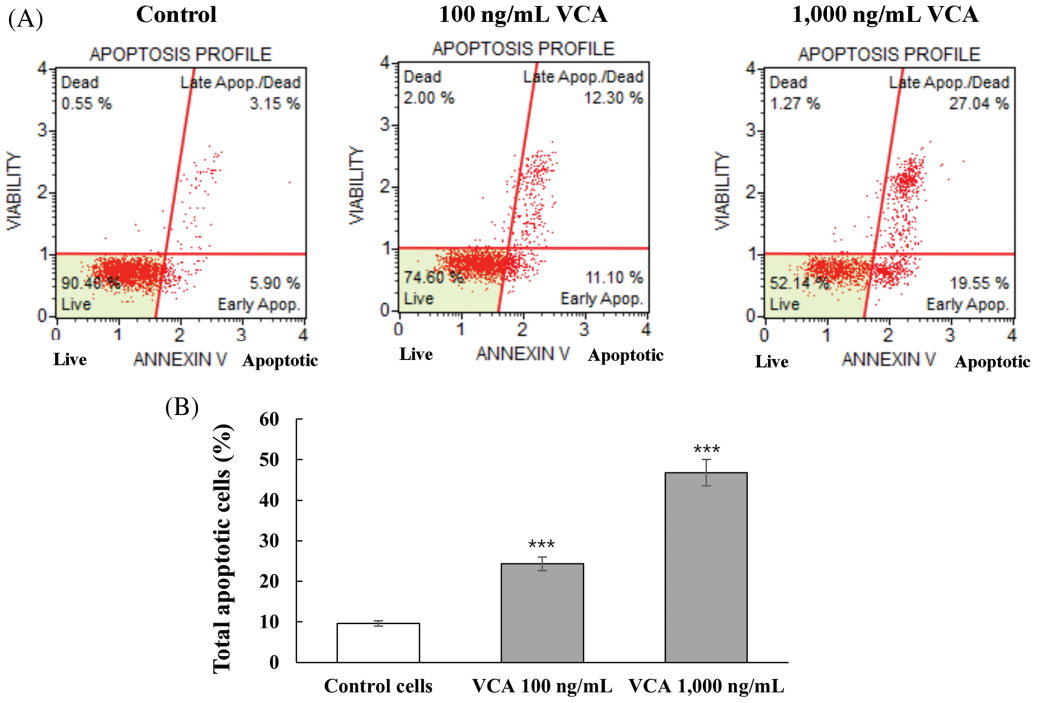


**Figure 2:** Evaluation of programmed cell death induction in YD38 oral cancer cells by *Viscum album* var. *coloratum* agglutinin (VCA). Experimental cultures were maintained in the presence of VCA (100 or 1000 ng/mL) for a 48-h duration, followed by dual-parameter flow cytometric detection utilizing Annexin V and 7-aminoactinomycin D (7-AAD) fluorescence markers. (A) Characteristic cytometric distribution patterns are displayed. (B) Quantification of total apoptotic cell populations. Numerical data represent mean ± standard deviation (SD) obtained from three replicate investigations. Asterisks indicate statistical difference from untreated controls: ***$p < 0.001$ (one-way ANOVA followed by Tukey's post-hoc test)

### 3.3 *Effect of VCA on Cell Cycle Distribution*

Flow cytometric examination of DNA content demonstrated that VCA exposure modifies cell cycle progression in YD38 cells (Fig. 3A,B). Distribution analysis of untreated populations showed 70.8 ± 1.1% cells in resting/early growth phase, 7.6 ± 0.4% in DNA synthesis phase, and 17.2 ± 0.6% in the mitotic preparation phase. Upon treatment with 100 ng/mL VCA, cells in the resting/early growth phase decreased to 55.9 ± 1.3% ($p < 0.001$), while DNA synthesis phase cells increased to 17.5 ± 0.7% ($p < 0.001$). A minor elevation to 17.8 ± 0.5% was observed in the mitotic preparation phase ($p > 0.05$). Higher concentration exposure (1000 ng/mL) intensified these shifts, with the resting/early growth phase further declining to 47.8 ± 1.5% ($p < 0.001$), DNA synthesis phase expanding to 24.3 ± 0.8% ($p < 0.001$), and mitotic preparation phase rising to 20.5 ± 0.7% ($p < 0.01$).

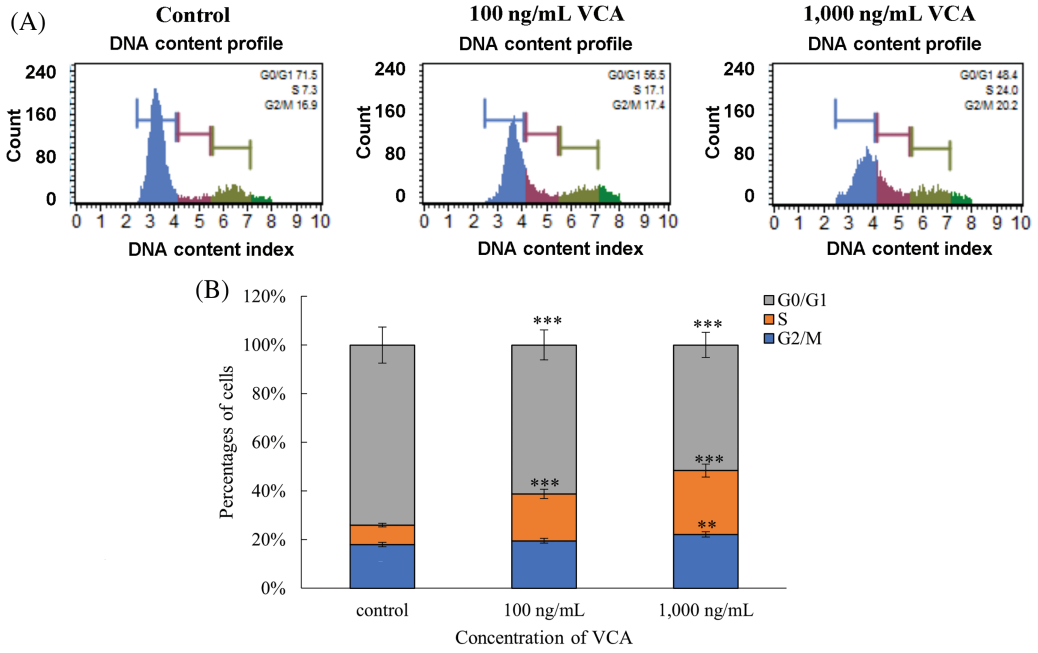


**Figure 3:** Analysis of cellular distribution across phases following *Viscum album* var. *coloratum* agglutinin (VCA) exposure. YD38 oral cancer cells underwent treatment with VCA at two concentrations (100 and 1000 ng/mL) maintained for 48 h, followed by nuclear DNA quantification through flow cytometric measurement using propidium iodide (PI) fluorescence. (A) Nuclear DNA content distribution profiles are presented. (B) Percentage distribution of cell populations within G0/G1, S, and G2/M compartments. Results show mean ± standard deviation (SD) derived from three independent experimental replicates. Significant variations from baseline controls are marked: $^{**}p < 0.01$, $^{***}p < 0.001$ (one-way ANOVA followed by Tukey's post-hoc test)

### 3.4 *VCA Modulates the Expression of Proteins Associated with Apoptosis*

Western blot analysis was carried out to examine the production of key proteins associated with apoptosis. Fig. 4A presents representative immunoblots of cleaved PARP (89 kDa), total caspase-3 (30 kDa), cleaved caspase-3 (17 kDa), and GAPDH (38 kDa) in YD38 cells treated with 100 and 1000 ng/mL VCA for 48 h. Densitometric analysis of the blots (Fig. 4B) revealed dose-dependent changes in protein expression levels. Cleaved PARP levels increased significantly with VCA treatment.

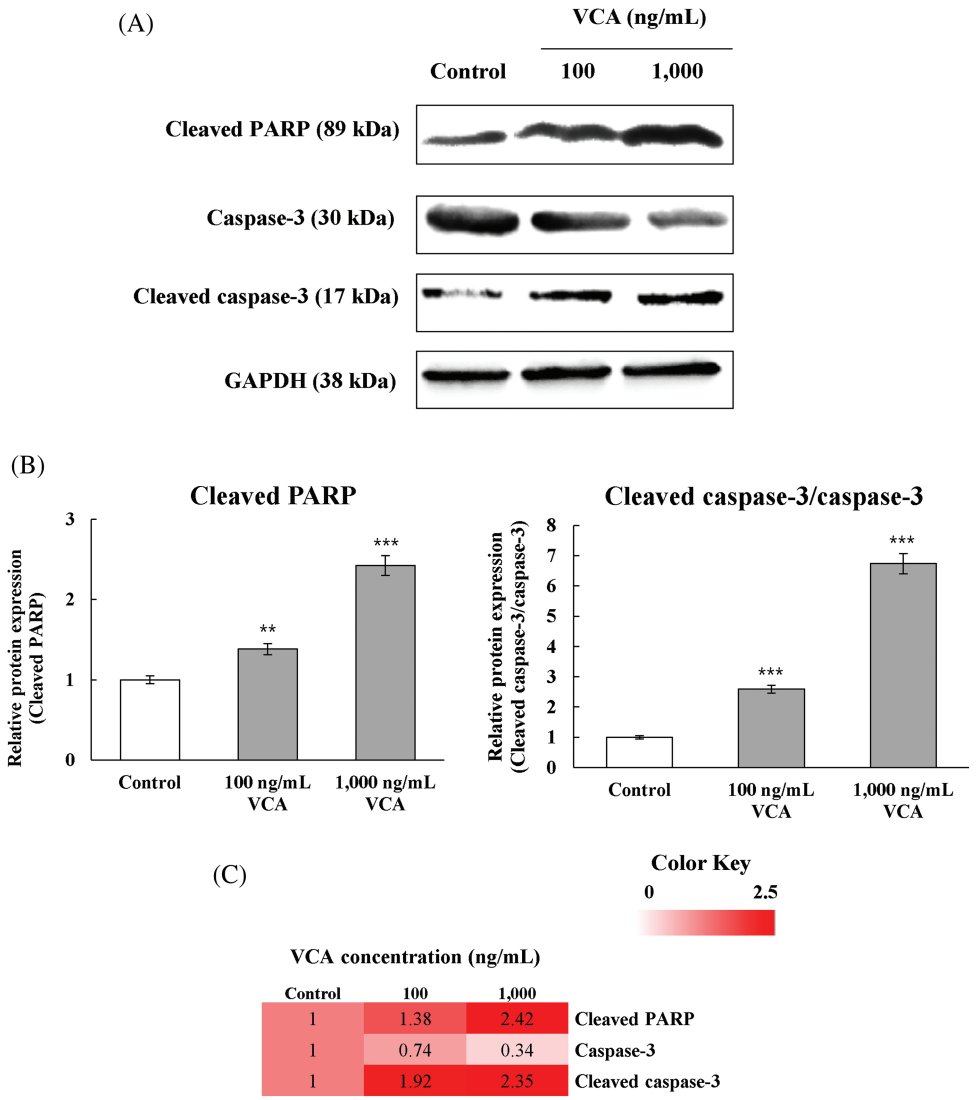


**Figure 4:** Molecular examination of cell death pathway proteins in YD38 oral cancer cells following *Viscum album* var. *coloratum* agglutinin (VCA) treatment. (A) Immunoblot visualization demonstrating proteolytic fragments of poly (ADP-ribose) polymerase (PARP, 89 kDa), caspase-3 (30 kDa), and its active form (17 kDa). Glyceraldehyde-3-phosphate dehydrogenase (GAPDH, 38 kDa) served as the internal normalization standard. (B) Densitometric quantitation of protein abundance. Cell samples were exposed to VCA (100 or 1000 ng/mL) for 48 h. Values indicate mean ± standard deviation (SD) from three independent biological replicates. Statistical analysis employed one-way ANOVA with subsequent Tukey's post-hoc comparison. $^{**}p < 0.01$, $^{***}p < 0.001$ vs. untreated controls. (C) Intensity gradient visualization depicting protein level alterations under experimental conditions. Color intensity correlates with $\log_2$-transformed fold change relative to baseline

At 100 ng/mL VCA, cleaved PARP increased to 1.38 ± 0.07-fold ($p < 0.01$) compared to the control. At 1000 ng/mL VCA, the increase was more substantial, reaching 2.42 ± 0.22-fold ($p < 0.001$) of the control level. Total caspase-3 levels showed a slight decrease with VCA treatment. At 100 ng/mL VCA, total caspase-3 decreased to 0.74 ± 0.11-fold of the control ($p < 0.05$). At 1000 ng/mL VCA, the decrease was more pronounced, reaching 0.34 ± 0.28-fold ($p < 0.01$) of the control level. Cleaved caspase-3 levels showed a significant increase with VCA treatment. At 100 ng/mL VCA, cleaved caspase-3 increased to 1.91 ± 0.43-fold

($p < 0.01$) of the control. The increase was more significant at 1000 ng/mL VCA, reaching 2.35 ± 0.65-fold ($p < 0.001$) of the control level. The ratio of cleaved caspase-3 to total caspase-3 was determined to assess the extent of caspase-3 activation. This ratio increased from 1 in control cells to 2.59 ± 0.15 ($p < 0.001$) in cells treated with 100 ng/mL VCA, and further increased to 6.73 ± 0.54 ($p < 0.001$) in cells treated with 1000 ng/mL VCA. These alterations in protein production levels correlate with the apoptotic effects of VCA observed in the flow cytometry experiments. To better visualize these coordinated changes in protein expression patterns, we generated a heatmap representation of the fold changes in protein levels relative to control (Fig. 4C), which clearly illustrates the dose-dependent upregulation of apoptotic markers and downregulation of total caspase-3 following VCA treatment.

### *3.5 Quantitative Assessment of VCA Effects on YD38 Cellular Processes*

One-way ANOVA revealed that VCA concentration had a significant effect on cell viability ($F(4, 10) = 79.23$, $p < 0.0001$), apoptosis induction ($F(2, 6) = 154.7$, $p < 0.0001$), and cell cycle distribution in G0/G1 ($F(2, 6) = 34.89$, $p = 0.0005$), S phase ($F(2, 6) = 45.67$, $p = 0.0002$), and G2/M phase ($F(2, 6) = 38.92$, $p = 0.0004$) (Fig. 5A,B and Table 1). Effect size calculations demonstrated very large effects of VCA treatment (1000 ng/mL) compared to control for cell viability (Cohen's $d = 7.08$), apoptosis induction (Cohen's $d = 30.24$), and G0/G1 phase distribution (Cohen's $d = 17.56$), S phase (Cohen's $d = 26.41$), and G2/M phase (Cohen's $d = 5.06$). A significant negative association was seen between cell viability and apoptosis rate ($r = -0.9997$, $p = 0.0145$), cell viability and S phase ($r = -0.981$, $p = 0.0189$), as well as G2/M phase ($r = -0.947$, $p = 0.0207$), indicating that the decrease in cell viability is closely associated with increased apoptosis and cell cycle modulation.

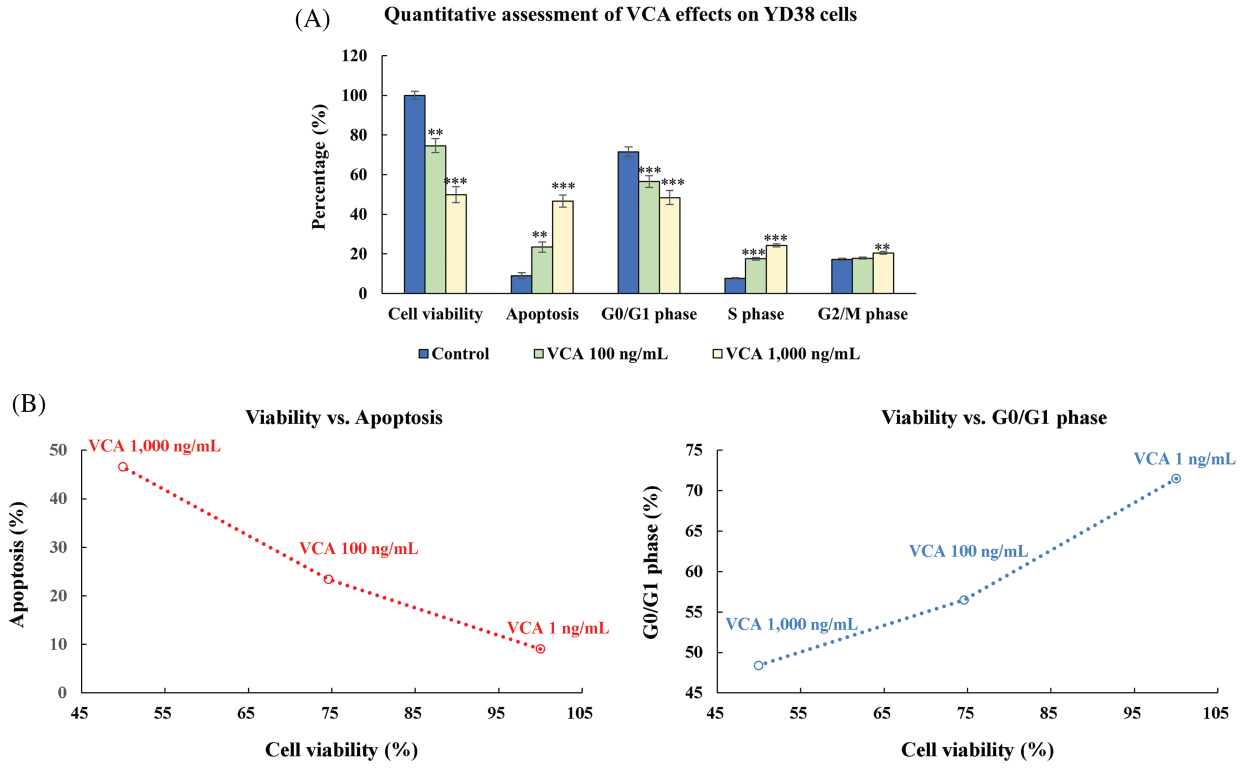


**Figure 5:** (Continued)

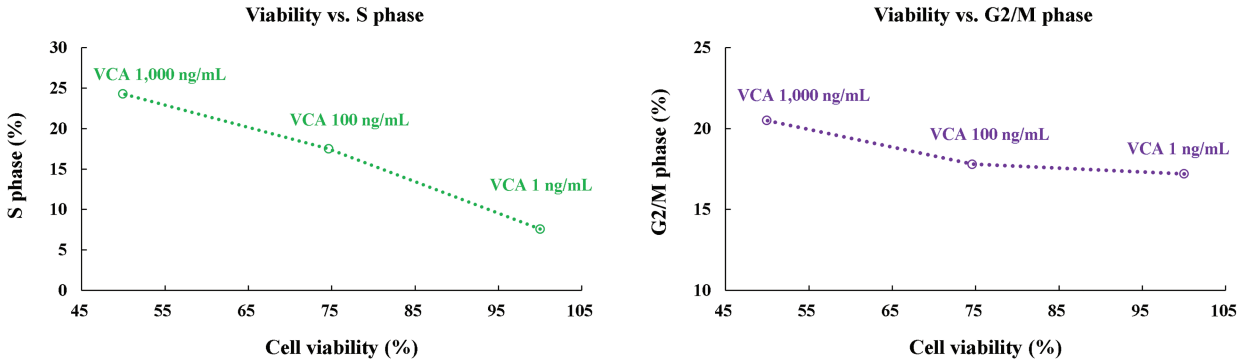


**Figure 5:** Integrated evaluation of multiple cellular responses to *Viscum album* var. *coloratum* agglutinin (VCA) in YD38 cells. Cell populations were exposed to VCA (0, 100, or 1000 ng/mL) over 48 h. (A) Graphical representation summarizing metabolic activity (3-(4,5-dimethylthiazol-2-yl)-2,5-diphenyltetrazolium bromide, MTT assay), cell death indicators (Annexin V/7-aminoactinomycin D, 7-AAD labeling), and cell cycle phase distribution (propidium iodide, PI fluorescence). Values display mean ± standard deviation (SD) derived from three independent experimental series. Significance levels vs. control group: $^{**}p < 0.01$, $^{***}p < 0.001$ (one-way ANOVA followed by Tukey's post-hoc test). (B) Matrix analysis revealing interrelationships among cellular parameters: metabolic status, programmed cell death, and cell cycle progression in VCA-treated samples. The interconnected patterns demonstrate concentration-dependent relationships among cellular survival, death pathway activation, and cell cycle alterations

**Table 1:** Effect sizes (Cohen's *d*) and statistical significance of *Viscum album* var. *coloratum* agglutinin (VCA) treatment effects on YD38 cells. The table shows Cohen's *d* values comparing control vs. VCA-treated conditions (100 and 1000 ng/mL) for various cellular parameters. Effect sizes were calculated from three independent experiments ($n = 3$). Cohen's *d* values ≥ 0.8 indicate large effect sizes. All comparisons showed statistical significance by one-way ANOVA followed by Tukey's post-hoc test. Statistical significance: All parameters showed $p < 0.001$ compared to control

| Comparison | Cohen's *d* value |
|---|---|
| Cell viability (Control *vs*. 100 ng/mL) | 53.34 |
| Cell viability (Control *vs*. 1000 ng/mL) | 7.08 |
| Apoptosis (Control *vs*. 100 ng/mL) | 15.15 |
| Apoptosis (Control *vs*. 1000 ng/mL) | 30.24 |
| G0/G1 (Control *vs*. 100 ng/mL) | 12.42 |
| G0/G1 (Control *vs*. 1000 ng/mL) | 17.56 |
| S (Control *vs*. 100 ng/mL) | 17.37 |
| S (Control *vs*. 1000 ng/mL) | 26.41 |
| G2/M (Control *vs*. 100 ng/mL) | 1.09 |
| G2/M (Control *vs*. 1000 ng/mL) | 5.06 |

### *3.6 Dose-Response Analysis*

of VCA on YD38 cells, we performed dose-response analysis and developed predictive models (Fig. 6). The experimental dose-response curves demonstrate clear relationships between VCA concentration and cellular responses, including cell viability, apoptosis induction, and cell cycle phase distributions (G0/G1, S, and G2/M phases). All parameters showed strong dose-dependent responses ($R^2 > 0.95$), with the most pronounced effects observed at higher VCA concentrations. Cell viability decreased progressively with increasing VCA concentration, while apoptosis induction and cell cycle changes (decreased G0/G1, increased

S and G2/M phases) showed consistent concentration-dependent changes throughout the tested range. Notably, the S phase showed highly significant changes ($p < 0.001$) at both 100 and 1000 ng/mL, while the G2/M phase showed significant changes ($p < 0.01$) only at 1000 ng/mL.

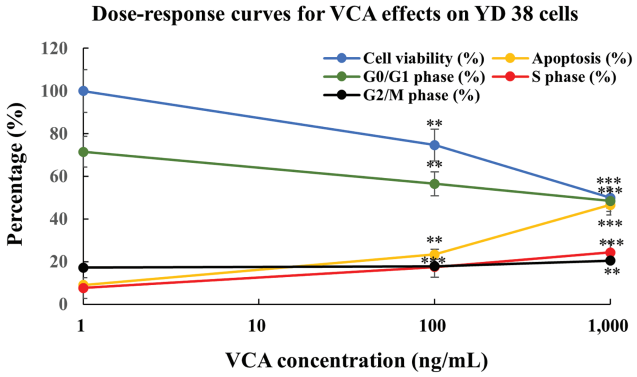


**Figure 6:** Concentration-dependent responses to *Viscum album* var. *coloratum* agglutinin (VCA) in YD38 cells. Quantitative relationship plots showing metabolic activity (blue), programmed cell death progression (yellow), and cell cycle phase distributions: G0/G1 (green), S (red), and G2/M (black). Each point represents mean ± standard deviation (SD) from three independent experimental series. The plotted curves illustrate the differential cellular parameter changes in response to increasing VCA levels. Markers denote significant differences from baseline: $^{**}p < 0.01$, $^{***}p < 0.001$ (one-way ANOVA with subsequent Tukey's post-hoc comparison). Mathematical modeling utilized non-linear regression fitting

### *3.7 Comprehensive Analysis of VCA Effects*

To comprehensively analyze VCA's effects across multiple cellular parameters, we first created a dual-axis representation combining all measured endpoints (Fig. 7A). This visualization revealed coordinated changes across cell viability, apoptosis, all cell cycle phases (G0/G1, S, and G2/M), and protein expression markers in response to increasing VCA concentrations. To understand the relationships between these various cellular responses, we performed correlation analysis (Fig. 7B), which revealed strong negative correlations between cell viability and apoptosis ($r = -0.997$) and between cell viability and cleaved PARP levels ($r = -0.994$). PCA was then conducted to evaluate the overall patterns in our multivariate dataset (Fig. 7C). The first two principal components explained 94.2% and 5.8% of the total variance, respectively, with a clear separation between control and VCA-treated samples along PC1, reflecting the dose-dependent nature of VCA's effects. Finally, to quantify the magnitude of VCA's effects, we calculated Cohen's $d$ values for key parameters comparing control vs. 1000 ng/mL treatment (Fig. 7D). All analyzed parameters showed large effect sizes ($d > 0.8$), with particularly strong effects observed for apoptosis induction and cell cycle modulation.

## 4 Discussion

In the present investigation, we looked into the anti-cancer properties of VCA on YD38 cells. Our findings demonstrate that VCA exhibits significant cytotoxicity against these cells, primarily via triggering of apoptosis and modulation of cell cycle progression.

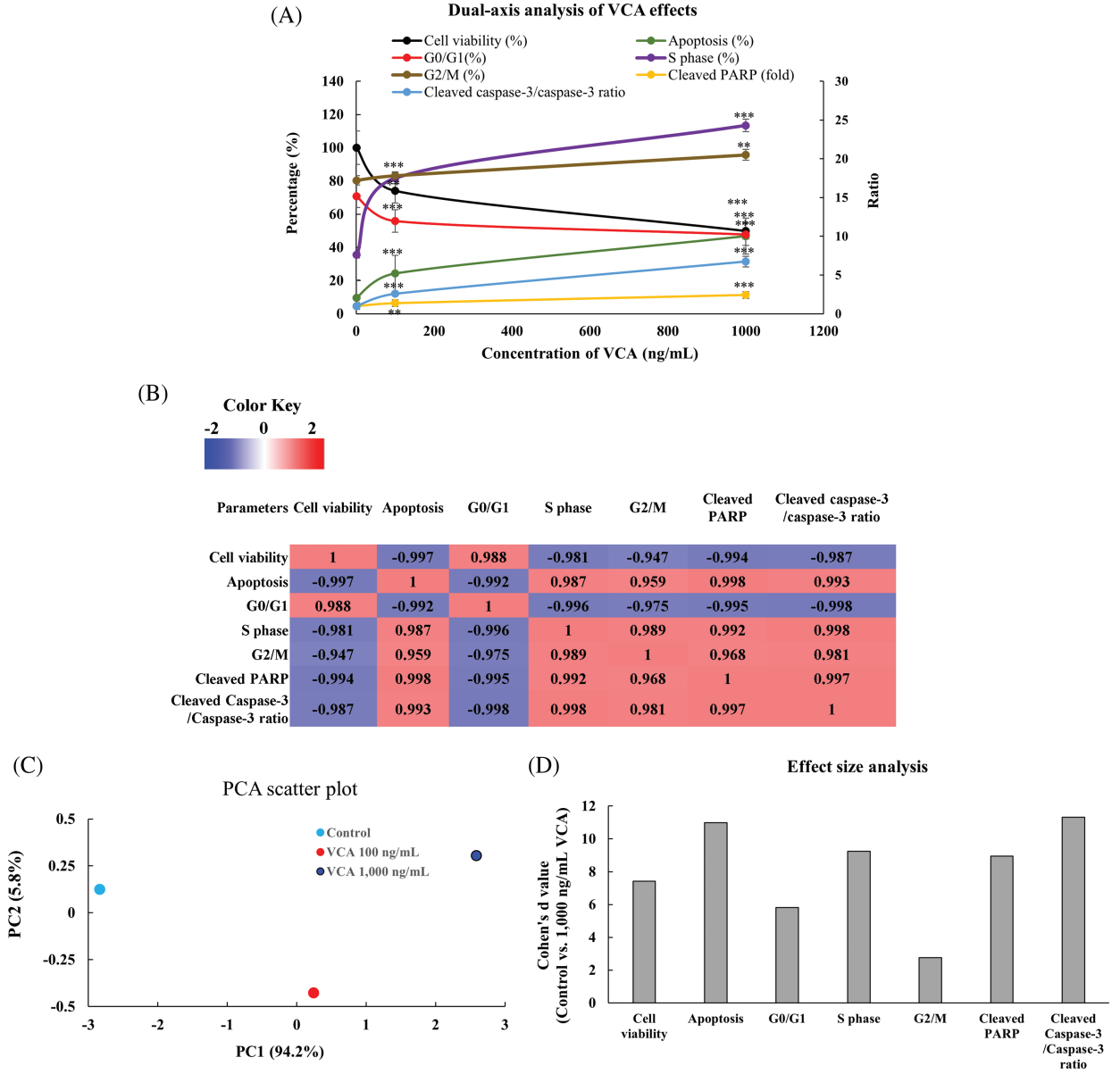


**Figure 7:** Comprehensive analysis of *Viscum album* var. *coloratum* agglutinin (VCA) effects on YD38 cells. (A) Dual-axis representation of VCA's concentration-dependent effects on cellular parameters. Left *Y*-axis shows percentage values for cell viability (black), apoptosis (green), G0/G1(red), S (purple), and G2/M (brown) phase distributions; Right *Y*-axis shows fold changes in cleaved PARP (yellow) and cleaved caspase-3/caspase-3 ratio (blue). Data are expressed as mean ± standard deviation (SD) of three separate studies. Statistical significance compared to control: $^{**}p < 0.01$, $^{***}p < 0.001$ (one-way ANOVA followed by Tukey's post-hoc test). (B) Symmetrical correlation matrix heatmap showing relationships between measured parameters. Correlation analyses were performed using data from control, 100 ng/mL, and 1000 ng/mL VCA treatments. Color intensity indicates correlation strength (red: positive association, blue: negative association). (C) Principal component analysis (PCA) plot showing the distribution of samples based on all measured parameters, with PC1 and PC2 explaining 94.2% and 5.8% of total variance, respectively. Different colors represent different VCA concentrations. (D) Effect size analysis showing Cohen's d values (with 95% confidence intervals) for key parameters comparing control *vs*. 1000 ng/mL VCA treatment. Vertical dashed lines indicate thresholds for small ($d$ = 0.2), medium ($d$ = 0.5), and large ($d$ = 0.8) effects. All observed effects exceeded the threshold for large effects ($d \geq 0.8$)

VCA showed potent dose-dependent cytotoxicity against YD38 cells after 48 h of treatment. The cytotoxic effect of VCA on YD38 cells observed in our study is comparable to its effects we previously reported in other cancer cell types. We previously demonstrated that VCA induced significant cytotoxicity in A253 submandibular gland squamous cell carcinoma cell line, at doses varying from 10 to 100 ng/mL [18]. This variation in sensitivity could be attributed to differences in cell surface glycosylation patterns or intracellular signaling pathways among different cancer types. Specifically, the higher sensitivity of A253 cells compared to YD38 cells might be due to differences in the expression levels of cell surface receptors that VCA binds to, or variations in the activity of pro-survival pathways between these cell lines [32]. For instance, YD38 cells harbor a p53 mutation [33], which could potentially affect their response to apoptotic stimuli induced by VCA. Also, the potency of VCA observed in our study is comparable to some conventional chemotherapeutic agents used in oral cancer treatment.

For instance, Khoo et al. reported an IC50 of 4.57 μM and 100 μM in H103 and H314 OSCC cell lines after cisplatin treatment, respectively [34]. Furthermore, our previous studies have demonstrated VCA's cytotoxic effects in multiple oral cancer cell lines including KB (mouth carcinoma) and FaDu (pharynx carcinoma) [31], supporting that VCA's anti-cancer properties are reproducible across different types of oral cancer cells. While direct comparisons should be made cautiously due to differences in experimental conditions, these findings suggest that VCA warrants further investigation as a potential therapeutic agent.

The apoptosis-inducing capability of VCA was confirmed through Annexin V/7-AAD staining, which revealed a significant increase in both early and late apoptotic populations at 100 and 1000 ng/mL VCA. The dose-dependent increase suggests that apoptosis is a primary mechanism by which VCA exerts its cytotoxic effects. At 1000 ng/mL VCA, the total apoptotic population increased to 46.8 ± 1.6% ($p < 0.001$), an approximately five-fold increase compared to untreated cells. This substantial increase in apoptotic cells correlates well with the observed decrease in cell viability, supporting the hypothesis that VCA-induced cell death is primarily mediated through apoptotic mechanisms.

The molecular process controlling VCA-induced apoptosis in YD38 cells was further elucidated by our Western blot analysis. The observed increases in cleaved PARP and cleaved caspase-3 levels indicate the triggering of the caspase-dependent apoptotic process. The cleavage of PARP, a DNA repair enzyme, is a hallmark of apoptosis and is primarily mediated by caspase-3 [35]. In our study, the significant increase in cleaved PARP levels (2.42 ± 0.22-fold at 1000 ng/mL VCA) indicates enhanced chromatin disassembly during programmed cell death. Additionally, executive phase proteolytic cascades were activated, as demonstrated by elevated cleaved caspase-3 levels (2.35 ± 0.65-fold at 1000 ng/mL VCA) and reduced total caspase-3 levels. The proportion of activated to zymogen caspase-3 increased from 1 in control cells to 6.73 ± 0.54 in cells treated with 1000 ng/mL VCA, providing a quantitative measure of caspase-3 activation. This substantial increase indicates a robust activation of the apoptotic machinery in response to VCA treatment, leading to the morphological and biochemical changes associated with apoptosis [36]. These findings are consistent with our previous studies on VCA. We previously reported increases in cleaved PARP and caspase-3 levels across several malignant cell types, particularly in salivary gland cancer cells, liver cancer cells, and hematologic cancer cells [37]. Similarly, Kim et al. demonstrated that VCA activated death signaling cascades in blood-derived malignant cells [38]. Also, these molecular changes are consistent with those reported for other plant-derived lectins. For example, Wu et al. found that *Polygonatum odoratum*-derived lectin initiated programmed cell death pathways in bronchial epithelial cancer cells [39]. Moreover, studies with *Kaempferia rotunda* plant protein demonstrated cytotoxic effects in intestinal tumor cells via modulation of caspase-3, -9, and PARP1 [40]. The similarity in molecular mechanisms across different lectins and cancer types suggests a conserved mode of action for these plant-derived compounds in inducing cancer cell apoptosis. While our study focuses on caspase-3 and PARP, the apoptotic cascade likely involves other molecular players. Previous

studies on mistletoe lectins have implicated the involvement of other caspases, B-cell lymphoma 2 (Bcl-2) family proteins, and mitochondrial pathways in the apoptotic process [18,37]. Further investigation into these additional molecular mechanisms in YD38 cells could provide a more comprehensive understanding of VCA's apoptosis-inducing effects.

Flow cytometric DNA content analysis demonstrated that VCA exposure modifies cell division patterns in YD38 cells. Phase distribution data revealed shifts toward DNA synthesis and mitotic preparation stages. Upon treatment with VCA (1000 ng/mL), cells in the DNA synthesis phase expanded from 7.6 ± 0.4% to 24.3 ± 0.8% ($p < 0.001$), while mitotic preparation phase populations rose from 17.2 ± 0.6% to 20.5 ± 0.7% ($p < 0.01$). These increases coincided with a reduction in resting phase cells from 70.8 ± 1.1% to 47.8 ± 1.5% ($p < 0.001$). This distribution profile shows distinct characteristics compared to our previous findings in salivary gland cancer models, where VCA primarily influenced DNA synthesis phase progression without affecting mitotic preparation [41]. This difference could be attributed to variations in the expression or activity of cell cycle regulators between YD38 [42,43] and A253 cells [44,45]. For example, YD38 cells might have different levels of cyclins or cyclin-dependent kinases that regulate the G2/M transition, leading to the observed accumulation in both S and G2/M phases. Similarly, we reported sub-G1 phase accumulation in B16BL6 melanoma cells treated with VCA [46]. The predominant sub-G1 accumulation in B16BL6 cells might indicate a higher susceptibility to VCA-induced apoptosis in these cells compared to YD38 cells, possibly due to differences in the intrinsic apoptotic machinery or the balance between pro-survival and pro-apoptotic factors.

Also, the cell cycle effects of VCA observed in our study differ somewhat from those reported for other mistletoe lectins. For instance, Siegle et al. found that mistletoe lectin I induced G1 phase arrest in A549 human lung carcinoma cells [47]. *Sophora flavescens* lectin was found to trigger G2/M phase arrest in MCF-7 human breast cancer cells through the upregulation of p21 and downregulation of cyclin-dependent kinase (CDK) 1 and 2 [48]. These differences highlight the potential for both cell type-specific and lectin-specific responses. The varying effects on cell cycle progression could be due to differences in the sugar-binding specificities of different lectins, leading to interactions with distinct cell surface receptors and subsequent activation of different intracellular signaling pathways [49]. Additionally, the genetic and epigenetic profiles of different cancer cell lines likely contribute to their unique responses to lectin treatment. This disparity highlights the potential for cancer type-specific responses to VCA and underscores the need for further investigation into the molecular mechanisms underlying these differences. Exploring the impact of VCA on similar cell cycle regulators in OSCC cells could provide valuable insights into its mode of action. This effect on cell cycle progression adds another dimension to VCA's anti-cancer mechanisms. Cell cycle arrest can prevent the proliferation of cancer cells and provide an opportunity for DNA repair or the initiation of apoptosis if the damage is irreparable [50]. The observed S and G2/M phase accumulation suggests that VCA may interfere with DNA synthesis and/or mitosis in YD38 cells.

The quantitative analyses further elucidated the potency and biological significance of VCA's effects on YD38 cells. The statistical analyses strongly support the biological significance of VCA's effects on YD38 cells. The large effect sizes observed for cell viability, apoptosis induction, and cell cycle modulation indicate that VCA exerts potent and meaningful biological effects. The strong negative correlation between cell viability and apoptosis rate suggests that VCA-induced cell death is primarily mediated through apoptotic mechanisms.

The dose-response analysis provides insights into the concentration-dependent effects of VCA on YD38 cells. Significant cellular changes were observed at VCA concentrations in the mid-to-high nanogram per milliliter range. Cell viability showed a consistent decrease with increasing VCA concentration, while G0/G1 phase distribution exhibited notable alterations at higher concentrations. The apoptotic response

demonstrated a progressive increase throughout the tested concentration range, with the most pronounced effects observed at higher concentrations. Our predictive models extend these observations, suggesting that the most dramatic changes in cell viability, apoptosis induction, and cell cycle distribution occur between 100 and 1000 ng/mL VCA. This finding aligns with previous studies on plant-derived lectins, which demonstrated comparable anti-proliferative activity across multiple cancer lineages [51–53].

The PCA and correlation analyses revealed important insights into the relationships between different cellular responses to VCA treatment. The strong separation of control and treated samples in the PCA plot, with the first principal component explaining 94.2% of the variance, indicates that VCA treatment induces a coordinated set of cellular responses. The strong correlations observed between different parameters (e.g., cell viability, apoptosis, and protein expression) suggest that these responses are mechanistically linked. For example, the strong negative correlation between cell viability and cleaved PARP levels ($r = -0.994$) provides quantitative support for the hypothesis that VCA-induced cell death occurs primarily through the activation of apoptotic pathways. These findings align with previous studies on plant lectins that have demonstrated coordinated cellular responses involving both cell cycle modulation and apoptotic pathway activation [47,51].

Our experimental observations suggest that VCA represents a promising therapeutic candidate for oral malignancies. The demonstrated capacity of VCA to trigger regulated cell death pathways and influence cellular replication dynamics in YD38 cells supports its development as an emerging oncology intervention. Our comprehensive statistical analyses, including effect size calculations and correlation studies, provide strong quantitative support for VCA's therapeutic potential. The large effect sizes observed for cell viability (Cohen's $d = 7.08$) and apoptosis induction (Cohen's $d = 30.24$) indicate highly significant biological effects. Furthermore, our dose-response analyses demonstrated potent activity of VCA in the nanogram range, with significant effects on both cell viability and cell cycle progression observed at relatively low concentrations. Given the challenges associated with current OSCC treatments, including drug resistance and severe side effects [54], natural compounds like VCA could offer alternative or complementary approaches. Moreover, the multi-faceted effects of VCA, including apoptosis induction and cell cycle modulation, could potentially address the issue of drug resistance often encountered in cancer therapy. The strong correlations observed between different cellular responses ($r > 0.95$) suggest a coordinated mechanism of action, which might help minimize the development of drug resistance. Combination therapies incorporating VCA with conventional chemotherapeutic agents might enhance treatment efficacy.

While our study provides valuable insights into the anti-cancer effects of VCA on OSCC, several limitations should be acknowledged. Firstly, this study was conducted *in vitro* using a single cell line (YD38). Future research should expand to include multiple OSCC cell lines and normal oral epithelial cells to better understand the specificity of VCA's effects. Additionally, while our predictive modeling suggests continued effects at higher concentrations, experimental validation beyond our tested range would be valuable. Secondly, the molecular mechanisms underlying VCA's effects on cell cycle progression require further elucidation. Detailed molecular analysis focusing on key cell division mediators, including phase-specific regulatory proteins and their associated kinase networks, would further elucidate the mechanisms underlying VCA's effects on cellular proliferation patterns. Thirdly, while we focused on the caspase-dependent apoptotic pathway, exploring other apoptotic pathways, such as the mitochondrial pathway and the role of Bcl-2 family proteins, could offer additional insights into VCA's mechanism of action. Finally, although our correlation analyses suggest coordinated cellular responses to VCA treatment, the causal relationships between these responses need to be further investigated.

## 5 Conclusion

This investigation demonstrates that VCA exhibits growth suppressive activities in YD38 oral carcinoma cells through multiple cellular pathways. The biological responses include activation of programmed cell death signaling, evidenced by enhanced PARP cleavage and modulation of caspase-3 processing. Additionally, the compound impacts cellular division patterns, particularly affecting DNA synthesis and mitotic progression phases. These concentration-dependent cellular responses align with our exploration of potential natural therapeutic candidates for oral cancer treatment. While these findings establish initial proof-of-concept for therapeutic application, additional validation using diverse oral cancer models and detailed mechanistic investigations will be essential to fully characterize the molecular basis of these observed effects.

**Acknowledgement:** None.

**Funding Statement:** The authors received no specific funding for this study.

**Author Contributions:** The authors confirm contribution to the paper as follows: study conception and design: Chang-Eui Hong and Su-Yun Lyu; data collection: Chang-Eui Hong; analysis and interpretation of results: Chang-Eui Hong and Su-Yun Lyu; draft manuscript preparation: Chang-Eui Hong and Su-Yun Lyu. All authors reviewed the results and approved the final version of the manuscript.

**Availability of Data and Materials:** The data that support the findings of this study are available from the corresponding author upon reasonable request.

**Ethics Approval:** Not applicable.

**Conflicts of Interest:** The authors declare no conflicts of interest to report regarding the present study.

**Appendix A**

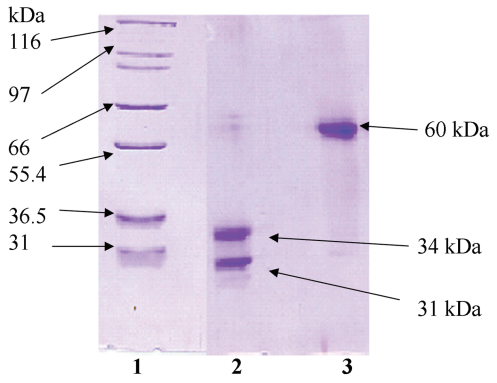


**Figure A1:** Electrophoretic characterization of Viscum album L. var. coloratum agglutinin (VCA) under different conditions. Protein fractions obtained through sequential purification using SP-50 Sephadex C-50 followed by asialofetuin-Sepharose 4B chromatography were subjected to SDS-PAGE analysis. Migration patterns were examined with (lane 2) and without (lane 3) reductive conditions. Reference molecular mass standards are shown in lane 1

## References

1. Siegel RL, Giaquinto AN, Jemal A. Cancer statistics, 2024. CA Cancer J Clin. 2024;74(1):12–49. doi:10.3322/caac.21820.

2. Li L, Tang D, Dai Y. The role of acetylation of histone H3 and H4 in oral squamous cell carcinoma. Oncologie. 2023;25(2):111–8. doi:10.1515/oncologie-2023-0071.
3. Ilie IO, Mărgăritescu OC, Stepan AE, Ciurea RN, Florescu MM, Munteanu C, et al. Epidemiological and histopathological features of oral squamous cell carcinoma-a retrospective study. Curr Health Sci J. 2024;50(5):411–20. doi:10.12865/chsj.50.03.08.
4. Das K, Gontu G, Aasumi K, Das RJ, Das A, Rahman T, et al. Occult metastasis: incidence, pattern, and impact on survival in patients with oral cancer, pN0 vs pN1 in a cohort of cN0. A prospective cohort study. Indian J Otolaryngol Head Neck Surg. 2024;76(6):5312–8. doi:10.1007/s12070-024-04968-2.
5. Dong L, Xue L, Cheng W, Tang J, Ran J, Li Y. Comprehensive survival analysis of oral squamous cell carcinoma patients undergoing initial radical surgery. BMC Oral Health. 2024;24(1):919. doi:10.1186/s12903-024-04690-z.
6. Ru L, Zheng J. Clinical applications and perspectives of immune checkpoint inhibitors in oral squamous cell carcinoma. Oncologie. 2024;26(4):535–47. doi:10.1515/oncologie-2024-0086.
7. Shah R, Shah H, Thakkar K, Parikh N. Conventional therapies of oral cancers: highlights on chemotherapeutic agents and radiotherapy, their adverse effects, and the cost burden of conventional therapies. Crit Rev Oncog. 2023;28(2):1–10. doi:10.1615/CritRevOncog.2023046835.
8. Biau J, Thivat E, Millardet C, Saroul N, Pham-Dang N, Molnar I, et al. A multicenter prospective phase II study of postoperative hypofractionated stereotactic body radiotherapy (SBRT) in the treatment of early-stage oropharyngeal and oral cavity cancers with high risk margins: the STEREO POSTOP GORTEC 2017-03 trial. BMC Cancer. 2020;20(1):730. doi:10.1186/s12885-020-07231-3.
9. Worthington HV, Bulsara VM, Glenny AM, Clarkson JE, Conway DI, Macluskey M. Interventions for the treatment of oral cavity and oropharyngeal cancers: surgical treatment. Cochrane Database Syst Rev. 2023;8(8):Cd006205. doi:10.1002/14651858.CD006205.pub5.
10. Siegel RL, Miller KD, Wagle NS, Jemal A. Cancer statistics, 2023. CA Cancer J Clin. 2023;73(1):17–48. doi:10.3322/caac.21763.
11. Newman DJ, Cragg GM. Natural products as sources of new drugs over the nearly four decades from 01/1981 to 09/2019. J Nat Prod. 2020;83(3):770–803. doi:10.1021/acs.jnatprod.9b01285.
12. Blanco Carcache PJ, Clinton SK, Kinghorn AD. Discovery of natural products for cancer prevention. Cancer J. 2024;30(5):313–9. doi:10.1097/PPO.0000000000000745.
13. Ghosh S, Das SK, Sinha K, Ghosh B, Sen K, Ghosh N, et al. The emerging role of natural products in cancer treatment. Arch Toxicol. 2024;98(8):2353–91. doi:10.1007/s00204-024-03786-3.
14. Nicoletti M. The antioxidant activity of mistletoes (*Viscum album* and Other Species). Plants. 2023;12(14):2707. doi:10.3390/plants12142707.
15. Yousefvand S, Fattahi F, Hosseini SM, Urech K, Schaller G. Viscotoxin and lectin content in foliage and fruit of *Viscum album* L. on the main host trees of Hyrcanian forests. Sci Rep. 2022;12(1):10383. doi:10.1038/s41598-022-14504-3.
16. Kang TB, Song SK, Yoon TJ, Yoo YC, Lee KH, Her E, et al. Isolation and characterization of two Korean mistletoe lectins. J Biochem Mol Biol. 2007;40(6):959–65. doi:10.5483/bmbrep.2007.40.6.959.
17. Park CH, Lee DW, Kang TB, Lee KH, Yoon TJ, Kim JB, et al. cDNA cloning and sequence analysis of the lectin genes of the Korean mistletoe (*Viscum album coloratum*). Mol Cells. 2001;12(2):215–20. doi:10.1016/S1016-8478(23)17086-5.
18. Khil LY, Kim W, Lyu S, Park WB, Yoon JW, Jun HS. Mechanisms involved in Korean mistletoe lectin-induced apoptosis of cancer cells. World J Gastroenterol. 2007;13(20):2811–8. doi:10.3748/wjg.v13.i20.2811.
19. Lee CH, Kim JK, Kim HY, Park SM, Lee SM. Immunomodulating effects of Korean mistletoe lectin *in vitro* and *in vivo*. Int Immunopharmacol. 2009;9(13–14):1555–61. doi:10.1016/j.intimp.2009.09.011.
20. Yoon TJ, Yoo YC, Kang TB, Song SK, Lee KB, Her E, et al. Antitumor activity of the Korean mistletoe lectin is attributed to activation of macrophages and NK cells. Arch Pharm Res. 2003;26(10):861–7. doi:10.1007/bf02980033.
21. Park HJ, Hong JH, Kwon HJ, Kim Y, Lee KH, Kim JB, et al. TLR4-mediated activation of mouse macrophages by Korean mistletoe lectin-C (KML-C). Biochem Biophys Res Commun. 2010;396(3):721–5. doi:10.1016/j.bbrc.2010.04.169.

22. Lee EJ, Kim J, Lee SA, Kim EJ, Chun YC, Ryu MH, et al. Characterization of newly established oral cancer cell lines derived from six squamous cell carcinoma and two mucoepidermoid carcinoma cells. Exp Mol Med. 2005;37(5):379–90. doi:10.1038/emm.2005.48.
23. Chen MM, Li J, Mills GB, Liang H. Predicting cancer cell line dependencies from the protein expression data of reverse-phase protein arrays. JCO Clin Cancer Inform. 2020;4(4):357–66. doi:10.1200/CCI.19.00144.
24. Pacini C, Duncan E, Gonçalves E, Gilbert J, Bhosle S, Horswell S, et al. A comprehensive clinically informed map of dependencies in cancer cells and framework for target prioritization. Cancer Cell. 2024;42(2):301–16. doi:10.1016/j.ccell.2023.12.016.
25. Jo DW, Kim YK, Yun PY. The influence of p53 mutation status on the anti-cancer effect of cisplatin in oral squamous cell carcinoma cell lines. J Korean Assoc Oral Maxillofac Surg. 2016;42(6):337–44. doi:10.5125/jkaoms.2016.42.6.337.
26. Ghandi M, Huang FW, Jané-Valbuena J, Kryukov GV, Lo CC, McDonald ER, et al. Next-generation characterization of the Cancer Cell Line Encyclopedia. Nature. 2019;569(7757):503–8. doi:10.1038/s41586-019-1186-3.
27. Alessandrini L, Astolfi L, Daloiso A, Sbaraglia M, Mondello T, Zanoletti E, et al. Diagnostic, prognostic, and therapeutic role for angiogenesis markers in head and neck squamous cell carcinoma: a narrative review. Int J Mol Sci. 2023;24(13):10733. doi:10.3390/ijms241310733.
28. Yu H, Shu J, Li Z. Lectin microarrays for glycoproteomics: an overview of their use and potential. Expert Rev Proteomics. 2020;17(1):27–39. doi:10.1080/14789450.2020.1720512.
29. Oinam SD, Senjam SS, Kamei R, Hanjabam JS. The role of lectin as potential biomarker in ovarian cancer. Curr Pharm Biotechnol. 2022;23(4):478–85. doi:10.2174/1389201022666210625125506.
30. Tansey W, Li K, Zhang H, Linderman SW, Rabadan R, Blei DM, et al. Dose-response modeling in high-throughput cancer drug screenings: an end-to-end approach. Biostatistics. 2022;23(2):643–65. doi:10.1093/biostatistics/kxaa047.
31. Lyu SY, Rhim JY, Moon YS, Jung SH, Lee KY, Park WB. Antitumor activities of extract of Viscum album var. coloratum Modified with Viscum album var. coloratum Agglutinin. Nat Prod Sci. 2002;8(4):155–61.
32. Gorelik E, Galili U, Raz A. On the role of cell surface carbohydrates and their binding proteins (lectins) in tumor metastasis. Cancer Metastasis Rev. 2001;20(3–4):245–77. doi:10.1023/a:1015535427597.
33. Li XH, Li D, Liu C, Zhang MM, Guan XJ, Fu YP. p33ING1b regulates acetylation of p53 in oral squamous cell carcinoma via SIR2. Cancer Cell Int. 2020;20(1):398. doi:10.1186/s12935-020-01489-0.
34. Khoo XH, Paterson IC, Goh BH, Lee WL. Cisplatin-resistance in oral squamous cell carcinoma: regulation by tumor cell-derived extracellular vesicles. Cancers. 2019;11(8):1166. doi:10.3390/cancers11081166.
35. Curtin NJ, Szabo C. Poly(ADP-ribose) polymerase inhibition: past, present and future. Nat Rev Drug Discov. 2020;19(10):711–36. doi:10.1038/s41573-020-0076-6.
36. Svandova E, Lesot H, Sharpe P, Matalova E. Making the head: caspases in life and death. Front Cell Dev Biol. 2022;10:1075751. doi:10.3389/fcell.2022.1075751.
37. Lyu SY, Park WB, Choi KH, Kim WH. Involvement of caspase-3 in apoptosis induced by Viscum album var. coloratum agglutinin in HL-60 cells. Biosci Biotechnol Biochem. 2001;65(3):534–41. doi:10.1271/bbb.65.534.
38. Kim MS, So HS, Lee KM, Park JS, Lee JH, Moon SK, et al. Activation of caspase cascades in Korean mistletoe (*Viscum album* var. *coloratum*) lectin-II-induced apoptosis of human myeloleukemic U937 cells. Gen Pharmacol. 2000;34(5):349–55. doi:10.1016/s0306-3623(01)00072-6.
39. Wu L, Liu T, Xiao Y, Li X, Zhu Y, Zhao Y, et al. Polygonatum odoratum lectin induces apoptosis and autophagy by regulation of microRNA-1290 and microRNA-15a-3p in human lung adenocarcinoma A549 cells. Int J Biol Macromol. 2016;85:217–26. doi:10.1016/j.ijbiomac.2015.11.014.
40. Islam F, Gopalan V, Lam AKY, Kabir SR. Kaempferia rotunda tuberous rhizome lectin induces apoptosis and growth inhibition of colon cancer cells *in vitro*. Int J Biol Macromol. 2019;141:775–82. doi:10.1016/j.ijbiomac.2019.09.051.
41. Choi SH, Lyu SY, Park WB. Mistletoe lectin induces apoptosis and telomerase inhibition in human A253 cancer cells through dephosphorylation of Akt. Arch Pharm Res. 2004;27(1):68–76. doi:10.1007/BF02980049.

42. Nipin SP, Kang DY, Kim BJ, Joung YH, Darvin P, Byun HJ, et al. Methylsulfonylmethane induces G(1) arrest and mitochondrial apoptosis in YD-38 gingival cancer cells. Anticancer Res. 2017;37(4):1637–46. doi:10.21873/anticanres.11494.
43. Son HK, Kim D. Quercetin induces cell cycle arrest and apoptosis in YD10B and YD38 oral squamous cell carcinoma cells. Asian Pac J Cancer Prev. 2023;24(1):283–9. doi:10.31557/APJCP.2023.24.1.283.
44. Yin MB, Guo B, Vanhoefer U, Azrak RG, Minderman H, Frank C, et al. Characterization of protein kinase chk1 essential for the cell cycle checkpoint after exposure of human head and neck carcinoma A253 cells to a novel topoisomerase I inhibitor BNP1350. Mol Pharmacol. 2000;57(3):453–9. doi:10.1016/S0026-895X(24)26409-9.
45. Park SB, Kwon Jung W, Rae Kim H, Yu HY, Hwan Kim Y, Kim J. Esculetin has therapeutic potential via the proapoptotic signaling pathway in A253 human submandibular salivary gland tumor cells. Exp Ther Med. 2022;24(2):533. doi:10.3892/etm.2022.11460.
46. Park WB, Lyu SY, Kim JH, Choi SH, Chung HK, Ahn SH, et al. Inhibition of tumor growth and metastasis by Korean mistletoe lectin is associated with apoptosis and antiangiogenesis. Cancer Biother Radiopharm. 2001;16(5):439–47. doi:10.1089/108497801753354348.
47. Siegle I, Fritz P, McClellan M, Gutzeit S, Mürdter TE. Combined cytotoxic action of *Viscum album* agglutinin-1 and anticancer agents against human A549 lung cancer cells. Anticancer Res. 2001;21(4a):2687–91.
48. Shi Z, Chen J, Li CY, An N, Wang ZJ, Yang SL, et al. Antitumor effects of concanavalin A and Sophora flavescens lectin *in vitro* and *in vivo*. Acta Pharmacol Sin. 2014;35(2):248–56. doi:10.1038/aps.2013.151.
49. Hatakeyama T, Unno H. Functional diversity of novel lectins with unique structural features in marine animals. Cells. 2023;12(14):1814. doi:10.3390/cells12141814.
50. Chaudhry GE, Akim AM, Sung YY, Muhammad TST. Cancer and apoptosis. Methods Mol Biol. 2022;2543(7):191–210. doi:10.1007/978-1-0716-2553-8_16.
51. Konozy EHE, Osman MEM. Plant lectin: a promising future anti-tumor drug. Biochimie. 2022;202(Suppl 1):136–45. doi:10.1016/j.biochi.2022.08.002.
52. Rudra A, Li J, Shakur R, Bhagchandani S, Langer R. Addition to trends in therapeutic conjugates: bench to clinic. Bioconjug Chem. 2020;31(4):1209. doi:10.1021/acs.bioconjchem.0c00136.
53. Gautam AK, Sharma D, Sharma J, Saini KC. Legume lectins: potential use as a diagnostics and therapeutics against the cancer. Int J Biol Macromol. 2020;142(22):474–83. doi:10.1016/j.ijbiomac.2019.09.119.
54. Tan Y, Wang Z, Xu M, Li B, Huang Z, Qin S, et al. Oral squamous cell carcinomas: state of the field and emerging directions. Int J Oral Sci. 2023;15(1):44. doi:10.1038/s41368-023-00249-w.